Journal of Alloys and Compounds 509 (2011) 6899–6907

Contents lists available at ScienceDirect

Journal of Alloys and Compounds

journal homepage: www.elsevier.com/locate/jallcom

Phase stability of magnesium-rare earth binary systems from first-principles calculations

Xiaoma Tao[a,b], Yifang Ouyang[a,d,*], Huashan Liu[b], Yuanping Feng[c], Yong Du[d], Yuehui He[d], Zhanpeng Jin[b]

[a] Department of Physics, Guangxi University, Nanning 530004, PR China
[b] School of Materials Science and Engineering, Central South University, Changsha 410083, PR China
[c] Department of Physics, National University of Singapore, 119260, Singapore
[d] State Key Laboratory of Powder Metallurgy, Central South University, Changsha 410083, PR China

ARTICLE INFO

Article history:
Received 15 December 2010
Received in revised form 30 March 2011
Accepted 30 March 2011
Available online 6 April 2011

Keywords:
First-principles
Mg–RE alloys
Thermodynamic property
Electronic structure

ABSTRACT

The comprehensive investigation to cohesive properties of 344 intermetallic compounds in 17 Mg–RE (RE = Sc, Y, and Lanthanide elements) binary system has been carried out systematically in the framework of density-functional theory (DFT) type first-principles with the generalized gradient approximation (GGA). The calculated properties at present work; including total energy, enthalpy of formation, equilibrium volume, bulk modulus, and electronic structure, was consistent with the experimental data. It was convinced that both $D0_3$-Mg_3RE and B2-MgRE were stable compounds in Mg–RE systems except Mg_3Eu, Mg_3Yb and Mg_3Lu in Mg_3RE series and MgYb for B2-MgRE branch extracting from calculated results.

1. Introduction

Magnesium and magnesium alloys have been drawn considerable attention due to their unique physical and mechanical properties, especially, the attractive low density, high specific strength, Young's modulus and good stiffness. Nowadays, magnesium alloys not only have been regarded as a promising structure materials comparing with aluminum alloys and many commercial steels [1] in regular technological field but also have been adopted as the priority in the automobile and aircraft industry.

Among diverse magnesium alloys, rare earth doped ones were designed to overcome their inherent poor mechanical performance in elevated temperature. It is convinced that fine precipitated rare-earth-rich intermetallic compounds of high thermal stability distributing on the grain boundary are effective block to the movement of dislocation. It is the very reason that a small quantity of rare earth elements additions can lead to a fantastic improvement on high temperature mechanical properties and microstructures [2]. Recently, the long period stacking ordered (LPSO) structure has been observed in the Mg-based alloys, the ordered phase might be the potential strengthening precipitation in Mg alloy [3–5].

Therefore, the prediction of the formation of intermetallic compounds and their thermal stability is vital to the design of heat-resistant magnesium alloys. Multi-scale calculation and simulation including first-principles (FP) calculation in the framework of DFT theory, semi-empirical embedded atom method (EAM), Miedema theory and CALPHAD technology has been launched.

Although Niessen et al. [6] and Ouyang et al. [7] have successfully calculated thermodynamic properties of Mg–RE binary systems by Miedema theory, and some pieces of calculated results based on EAM [8] and FP have been apply to phase diagrams assessments of Mg–RE systems, for example Mg–Sc [9], Mg–Y [10], Mg–La [11], Mg–Ce [12], Mg–Pr [13], Mg–Nd [14], Mg–Eu [15], Mg–Gd [16], Mg–Tb [17], Mg–Dy [16], Mg–Ho [16], Mg–Er [18], Mg–Tm [19] and Mg–Yb [17]. However, no systematically investigation to thermodynamic properties of Mg–RE is available in reported literature.

Using the diffusion couple method, the intermetallic phases of Mg–Ce have been investigated [20,21], and confirmed the compositions of the four binary intermetallics on the Mg-rich half as $Mg_{11}Ce$, $Mg_{39}Ce_5$, Mg_3Ce, and MgCe. The thermodynamic and electronic structures of Mg–Ce intermetallic compounds [22] have been calculated by using first-principles calculation. The enthalpies of formation of Mg–X (X = Y, La, Dy, and Lu) binary intermetallic compounds have been calculated by using first-principles [23], the enthalpies of formation of the Mg–La system have been determined

* Corresponding author at: Department of Physics, Guangxi University, Nanning 530004, PR China. Tel.: +86 771 3232208; fax: +86 771 3237386.
E-mail address: ouyangyf@gxu.edu.cn (Y. Ouyang).

0925-8388/$ – see front matter © 2011 Elsevier B.V. All rights reserved.
doi:10.1016/j.jallcom.2011.03.177

at 298 K by means of solution calorimetry [24], and the enthalpies of formation of Mg–La [25] also have been studied by first-principles calculation. Using first-principles calculation, the thermodynamic, elastic and electronic properties of Mg–Gd have been calculated [26].

The present study is aimed to obtain accurate formation enthalpies of all Mg–RE binary systems by first-principles calculation, including the RE-rich magnesium alloys, metastable phase and hypothetical phase, to enhance the accuracy when experimental data are not available.

In this paper, the first-principles method based on density functional theory is used to investigate thermodynamic properties and phase stability of Mg_3RE, Mg_2RE, MgRE, $MgRE_2$, $MgRE_3$ intermetallic compounds. The common structures, i.e. A15, $L1_2$, $D0_3$, $D0_{19}$, C1, C15, C14, $C11_b$, B1, B2, B3, and B32 structures has been calculated in the present calculation. Meanwhile, some stable phase of the Mg-rich RE phases are also taken into account in the present work (such as $Mg_{12}La$, $Mg_{17}La_2$). The calculated thermodynamic properties, phase stability and electronic structure will be presented in Section 3. Finally, in Section 4, we will present some general conclusions.

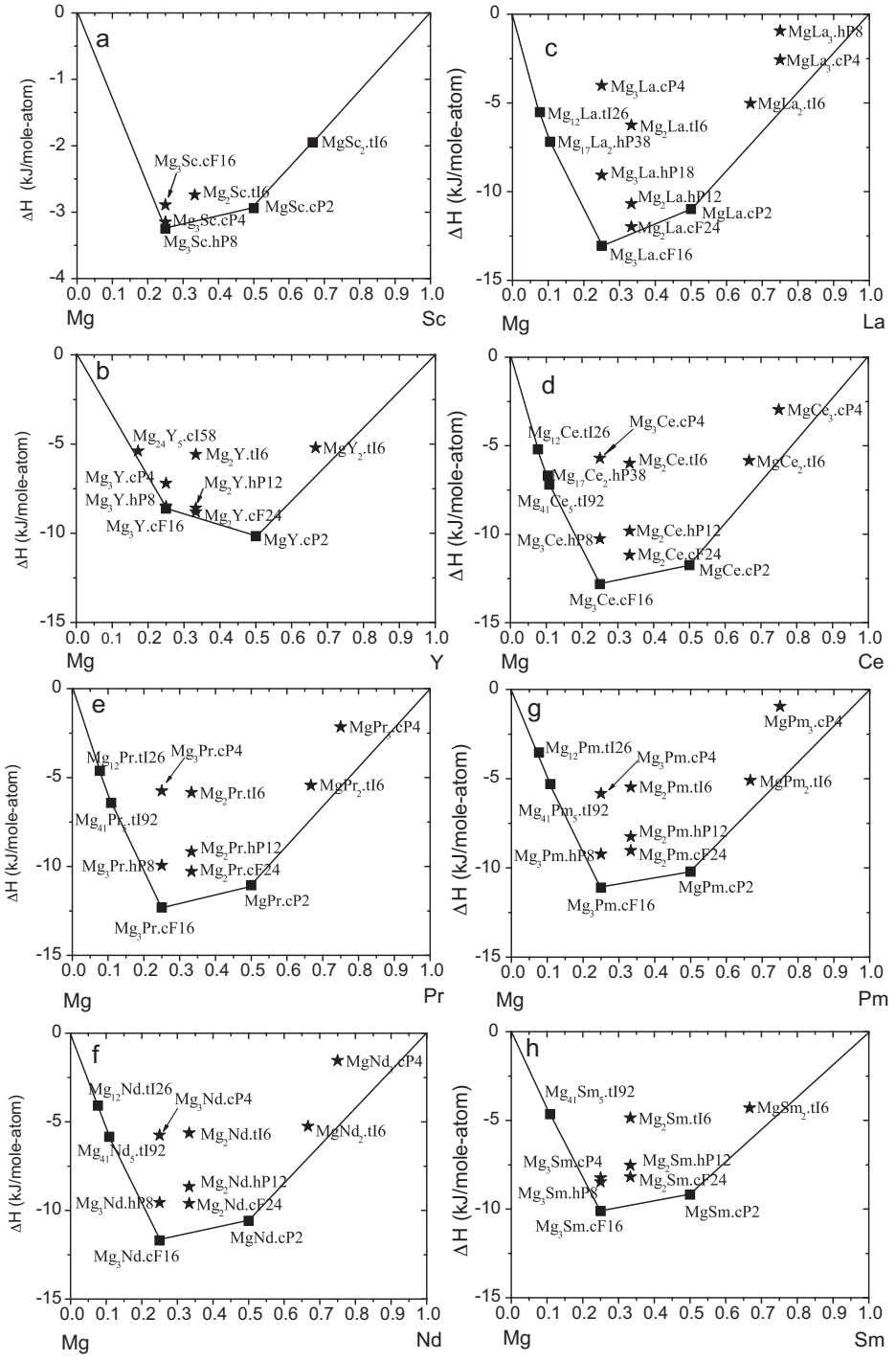

Fig. 1. The convex hull plots of the enthalpies of formation of Mg–RE (RE = Sc, Y, La, Ce–Lu) binary systems calculated at 0 K. The solid line defines the ground state convex hull.

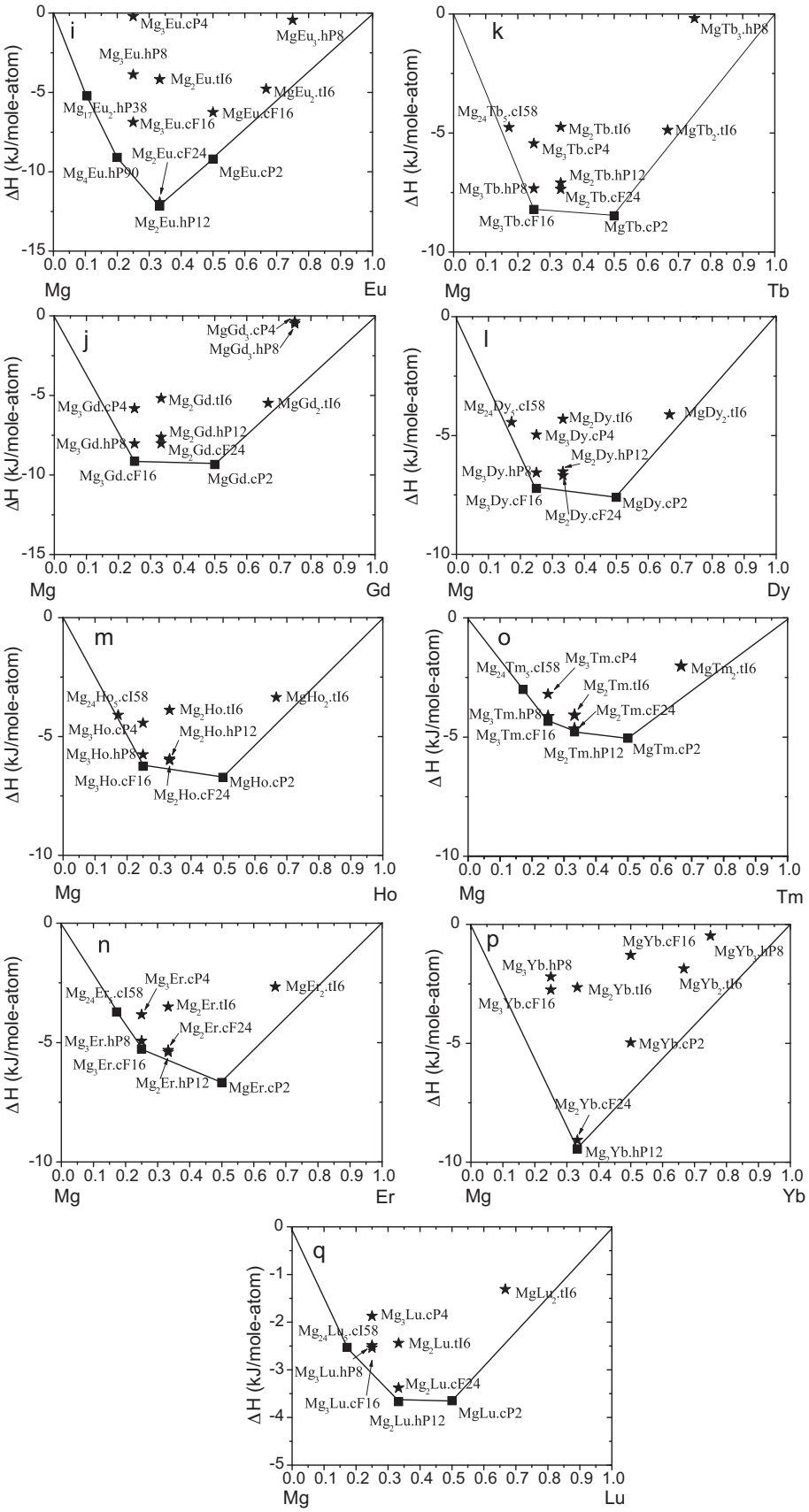

Fig. 1. (*continued.*)

2. Computational methodology

First-principles calculations were performed by using the scalar relativistic all-electron Blöchl's projector augmented wave (PAW) approach [27,28] within the generalized gradient approximation (GGA), as implemented in the high-efficient Vienna *ab initio* simulation package (VASP) [29,30]. For the GGA exchange-correlation function, the Perdew–Wang parameterization (PW91) [31,32] was employed. A plane-wave energy cutoff of 350 eV was held constant for all the Mg_xRE_y compounds. The *k*-point meshes for Brillouin zone sampling were constructed using the Monkhorst–Pack scheme [33] and the *k*-points meshes are increased to achieve convergence to a precision of better than 5 meV/atom. The total energy was converged to less than 1×10^{-6} eV/cell. Optimization of lattice structures was performed for each structure; the considered structures were fully relaxed until the forces on all the atoms were less than 0.01 eV/Å. All calculations are performed using the "PREC = high" setting within the VASP to avoid wrap-around errors. Spin polarization was used in all calculations. In addition, using the PW91-Tm_3 potential, the total energy cannot converge with a complex cell for the Tm element or Tm-bearing alloys, such as the FCC, Sm-type structures, and $D0_3$($L1_2$, $D0_{19}$)-$MgTm_3$. In order to obtain the completely thermodynamic data for the Mg–Tm, the PBE potential of the Tm_3 was employed in the above structures.

Note that the potpaw-GGA-PW91 potentials of Mg, Sc, Y_sv, La, RE_3(RE = Ce, Pr, Nd, Pm, Sm, Gd, Tb, Dy, Go, Er, Tm, Lu), Eu_2, Yb_2 and the potpaw-GGA-PBE potential of Tm_3 were used in the present work.

In order to obtain the equilibrium unit cell volume, the total energy calculations were performed for each structure with a set of volumes, with all atoms occupying their ideal lattice sites. Those total energies as a function of volume were then fitted to the Vinet's equation of state [34]. And then the equilibrium volume, total energy, bulk modulus and its pressure derivative $(\partial B/\partial P)_T$ were evaluated.

The formation enthalpy for Mg_xRE_y alloys was calculated by the following equation:

$$\Delta H(Mg_xRE_y) = E_{total}(Mg_xRE_y) - xE_{total}(Mg) - yE_{total}(RE) \quad (1)$$

where $E_{total}(Mg_xRE_y)$, $E_{total}(Mg)$, and $E_{total}(RE)$ are calculated total energies (per atom at $T = 0$ K) for Mg_xRE_y compounds, Mg and RE, respectively. During calculation, Ce, and Yb are of FCC structure, Eu of BCC structure, La, Pr, Nd, Pm and Sm with dHCP structure, and Mg, Sc, Y, Gd, Tb, Dy, Ho, Er, Tm, Lu with HCP structure.

3. Results and discussion

3.1. Enthalpies of formation, equilibrium volume and bulk modulus

The calculated enthalpies of formation for the 344 binary Mg–RE phases and the available experimental values have been listed in Tables 1 and 2, respectively. The calculated enthalpies of formation of the binary Mg–RE systems have also been displayed in Fig. 1 and equilibrium volume for Mg–RE systems are illustrated in Fig. 2 compared with experimental values and other available theoretical values. In general, the present calculated results agree well with experimental data [35–37], described in detail as following.

3.1.1. Mg–Sc and Mg–Y

From Fig. 1(a), the enthalpies of formation of Mg_3Sc.hP8, MgSc.cP2 and $MgSc_2$.tI6 lie on the convex hull, and only the MgSc.cP2 is the stable phase in experiment [35,36]. Mg_3Sc.hP8 and $MgSc_2$.tI6 lie on the convex hull, which indicated the Mg_3Sc.hP8 and $MgSc_2$.tI16 are stable phases at 0 K in the present calculations.

Table 1
The calculated enthalpies of formation of Mg–RE bianry system.

Phase	Prototype	*Strukturbericht* symbols	Sc	Y	La	Ce	Pr	Nd	Pm	Sm	Eu	Gd	Tb	Dy	Ho	Er	Tm	Yb	Lu
$Mg_{24}RE_5$	αMn.cI58	A12	–	−5.4	–	–	–	–	–	–	–	–	−4.8	−4.4	−4.1	−3.7	−3.0	–	−2.5
$Mg_{12}RE$	$Mn_{12}Th$.tI26	$D2_b$	–	–	−5.5	−5.2	−4.6	−4.1	−3.5	–	–	–	–	–	–	–	–	–	–
$Mg_{17}RE_2$	$Ni_{17}Th_2$.hP38	–	–	–	−7.2	−6.7	–	–	–	–	−5.2	–	–	–	–	–	–	–	–
$Mg_{41}RE_5$	$Mg_{41}Ce_5$.tI92	–	–	–	–	−7.0	–	–	–	−4.7	–	–	–	–	–	–	–	–	–
Mg_4RE	Mg_4Sr.hP90	–	–	–	–	–	–	–	–	–	−9.1	–	–	–	–	–	–	–	–
Mg_3RE	Cr_3Si.cP8	A15	12.1	8.1	6.4	5.8	6.2	6.6	6.9	7.6	5.2	7.8	8.4	9.0	9.5	10.0	10.4	6.5	11.3
Mg_3RE	$AuCu_3$.cP4	$L1_2$	−3.1	−7.2	−4.0	−5.7	−5.8	−5.7	−5.8	−8.2	−0.2	−5.8	−5.4	−5.0	−4.4	−3.8	−3.2	0.1	−1.9
Mg_3RE	BiF_3.cF16	DO_3	−2.9	−8.6	−13.1	−12.8	−12.3	−11.7	−11.1	−10.1	−6.9	−9.1	−8.2	−7.2	−6.2	−5.3	−4.3	−2.7	−2.5
Mg_3RE	Ni_3Sn.hP8	DO_{19}	−3.3	−8.5	−9.1	−10.2	−9.9	−9.6	−9.2	−8.5	−3.9	−8.0	−7.3	−6.6	−5.8	−4.9	−4.1	-2.2	−2.5
Mg_2RE	CaF_2.cF12	C1	53.4	50.6	43.7	42.2	43.8	45.4	46.8	48.5	41.2	50.3	51.5	52.6	53.6	54.5	55.2	42.1	56.3
Mg_2RE	$MgZn_2$.hP12	C14	2.9	−8.6	−10.7	−9.8	−9.2	−8.7	−8.2	−7.5	−12.2	−7.6	−7.1	−6.5	−5.9	−5.4	−4.8	−9.4	−3.7
Mg_2RE	$MgCu_2$.cF24	C15	3.3	−8.8	−12.0	−11.2	−10.3	−9.6	−9.0	−8.2	−11.9	−8.0	−7.4	−6.7	−6.0	−5.3	−4.7	−9.1	−3.4
Mg_2RE	$MoSi_2$.tI6	$C11_b$	−2.7	−5.6	−6.2	−6.0	−5.8	−5.6	−5.5	−4.9	−4.2	−5.2	−4.8	−4.3	−3.9	−3.5	−4.1	−2.7	−2.4
MgRE	NaCl.cF8	B1	44.1	33.1	35.0	33.1	33.9	34.5	34.9	35.9	23.7	36.1	37.1	38.4	39.8	41.3	42.8	27.7	45.8
MgRE	CsCl.cP2	B2	−3	−10.2	−11	−12	−11	−11	−10	−9	−9	−9.3	−8.5	−7.6	−6.7	−6.7	−5.1	−5.0	−3.7
MgRE	ZnS.cF8	B3	128.4	115.5	103.3	104.5	107.5	110.0	112.1	114.1	69.7	116.2	117.6	118.8	119.8	120.7	121.4	70.9	122.0
MgRE	NaTl.cF16	B32	7.4	8.2	8.4	10.7	10.9	10.9	10.4	10.3	−6.3	8.0	7.7	7.4	7.1	6.9	6.5	−1.3	5.8
$MgRE_2$	CaF_2.cF12	C1	52.4	37.4	31.4	32.0	33.9	35.3	36.4	37.9	16.7	38.1	39.0	40.0	40.8	41.6	42.3	18.7	43.4
$MgRE_2$	$MgCu_2$.cF24	C15	19.2	28.6	24.6	27.8	27.3	27.0	26.7	27.3	26.6	25.5	25.7	25.9	26.1	26.2	26.2	25.7	26.1
$MgRE_2$	$MoSi_2$.tI6	$C11_b$	−2.0	−5.2	−5.0	−5.8	−5.4	−5.2	−5.1	−4.3	−4.8	−5.5	−4.9	−4.2	−3.4	−2.7	−2.0	−1.9	−1.3
$MgRE_3$	Cr_3Si.cP8	A15	8.6	7.1	5.5	5.7	6.5	7.0	7.4	8.6	4.5	7.5	8.1	8.7	9.3	9.7	10.1	5.0	10.7
$MgRE_3$	$AuCu_3$.cP4	$L1_2$	3.8	1.7	−2.6	−3.0	−2.1	−1.5	−0.9	0.4	1.1	−0.3	0.5	1.4	2.2	2.9	4.4	1.0	4.2
$MgRE_3$	BiF_3.cF16	DO_3	6.7	5.6	5.1	4.6	4.9	4.9	4.9	5.7	0.5	3.9	4.3	4.7	5.1	5.5	6.6	1.1	5.8
$MgRE_3$	Ni_3Sn.hP8	DO_{19}	1.9	−0.1	−1	−0.4	0.2	0.5	0.6	1.4	−0.4	−0.5	−0.2	0.2	0.5	0.9	1.9	−0.5	1.5

Table 2
The experimental enthalpies of formation of Mg–RE binary system.

RE	MgRE	Mg_2RE	Mg_3RE	$Mg_{24}RE_5$	$Mg_{41}RE_5$	$Mg_{12}RE$	Reference
Y	−12.6	−14.2	–	-7.53	–	–	[38]
	−30.3	−12.0	–	−6.1	–	–	[39]
	–	−17.7	–	–	–	–	[40]
Ce	−13.1	−11.4	−18.9	–	−18.1	−14.1	[41]
Nd	−13.9	−18.7	−18.7	–	-18	−13.9	[41]
Gd	−17.4	−19.7	−19	–	−17	–	[41]
Dy	−12	−16.3	−16.1	−13.7	–	–	[41]
Er	−21.3	−22	–	−16.1	–	–	[41]
Lu	−35.7	−35.7	–	−25.2	–	–	[41]

The Mg_3Sc.cP4, Mg_3Sc.cF16 and Mg_2Sc.tI6 lie above the convex hull 0.10, 0.36, and 0.39 kJ/mol of atom, respectively. Those phases have not been reported in any literatures, but the present calculations show that they are close to the energy of stable phase.

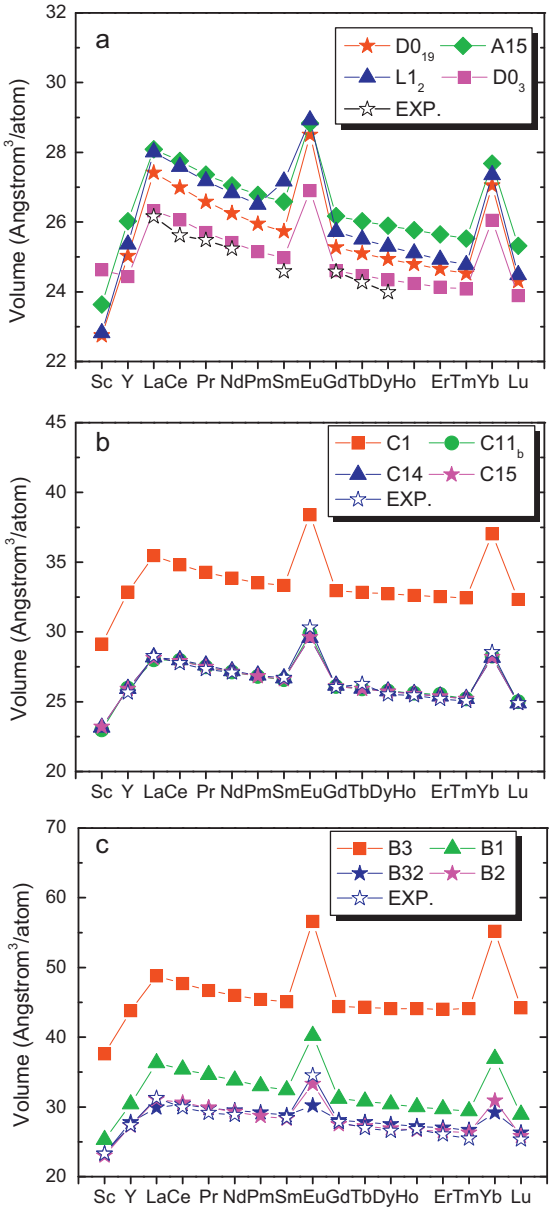

Fig. 2. The trend of the volume of three groups of intermetallic compounds across the periodic table: (a) Mg_3RE family, (b) Mg_2RE family, (c) MgRE family. The experimental volume of MgEu is taken from Ref. [37] and the others are taken from Ref. [36].

As for Mg–Y system (see Fig. 1(b)), the Mg_3Y.cF16 and MgY.cP2 lie on the convex hull, and MgY.cP2 is a stable phase observed in experiment [35,36], Mg_3Y.cF16 has not been detected by experiment. It will be noted that Mg_2Y.cF24 has a slightly lower formation enthalpy than that of Mg_2Y.hP12 phase, and they lie above the convex hull by 0.43 and 0.64 kJ/mol of atom, respectively. The $Mg_{24}Y_5$.cI58 lies above the convex hull by 0.40 kJ/mol of atom. The Mg_2Y.hP12 and $Mg_{24}Y_5$.cI58 are stable phases in experiment [35,36].

3.1.2. Mg–La and Mg–Ce

Fig. 1(c) shows that $Mg_{12}La$.tI26, $Mg_{17}La_2$.hP38 and Mg_3La.cF16 and MgLa.cP2 are stable phases. Mg_2La.cF24 is above the convex hull by 0.39 kJ/mol of atom, and it is stable at high temperature (998–1048 K) in experiment [35].

The results from Fig. 1(d) are shown that $Mg_{12}Ce$.tI26, $Mg_{17}Ce_2$.hP38, $Mg_{41}Ce_5$.tI92, Mg_3Ce.cF16 and MgCe.cP2 lie on the convex hull, and they are stable phases in experiment [35,36] except $Mg_{17}Ce_2$.hP38. According to the binary phase diagram [35], there is a phase denoted as $Mg_{10.3}Ce$. In this work, the $Mg_{17}Ce_2$.hP38 is fairly close to $Mg_{10.3}Ce$ and the $Mg_{17}Ce_2$.hP38 phase has been reported in Ref. [36], so the $Mg_{17}Ce_2$.hP38 phase has been calculated. From Table 1 and Fig. 1(d), the $Mg_{17}Ce_2$.hP38 phase lies on the convex hull, which indicates the stability of $Mg_{17}Ce_2$.hP38 at 0 K. The Mg_2Ce.cF24 lies above the convex hull by 1.26 kJ/mol of atom. It is explicit that Mg_2Ce.cF24 occupies the stable temperature range between 888 K and 1023 K [35].

3.1.3. Mg–Pr, Mg–Nd, Mg–Pm and Mg–Sm

From Fig. 1(e), $Mg_{12}Pr$.tI26, $Mg_{41}Pr_5$.tI92, Mg_3Pr.cF16 and MgPr.cP2 lie on the convex hull, and they are all stable phases observed in experiments [35,36]. Mg_2Pr.cF24 and $MgPr_2$.tI6 lie above the convex hull by 1.56 and 1.84 kJ/mol of atom, respectively. Mg_2Pr.cF24 is stable phase at high temperature [35], while $MgPr_2$.tI6 has not been reported in the literature.

And from Fig. 1(f)–(h), the Mg–Nd, Mg–Pm and Mg–Sm have similar tendency as that of the Mg–Pr system, namely, $Mg_{12}Nd$.tI26, $Mg_{41}Nd_5$.tI92, Mg_3Nd.cF16, MgNd.cP2, $Mg_{12}Pm$.tI26, $Mg_{41}Pm_5$.tI92, Mg_3Pm.cF16, MgPm.cP2, $Mg_{41}Sm_5$.tI92, Mg_3Sm.cF16 and MgSm.cP2 lie on the convex hull. Mg_2RE.cF24 structure is a high temperature phase [35] and $MgRE_2$.tI6 lies above the convex hull within 2.00 kJ/mol of atom. For the Mg_5Sm phase [35], the detailed crystal information has not been detected by experiment, so the Mg_5Sm has not been included in present work.

Although the phase diagram of Mg–Pm has not been determined experimentally, the calculations for this system have been carried out. Pm is a light rare earth element, located between Nd and Sm in the periodic table; therefore, its physical and chemical properties are similar to those of Nd and Sm. It is reasonable that three phase diagrams present the similar appearance. Form Fig. 1(g), $Mg_{12}Pm$.tI26, $Mg_{41}Pm_5$.tI92, Mg_3Pm.cF16, and MgPm.cP2 lie on the convex hull.

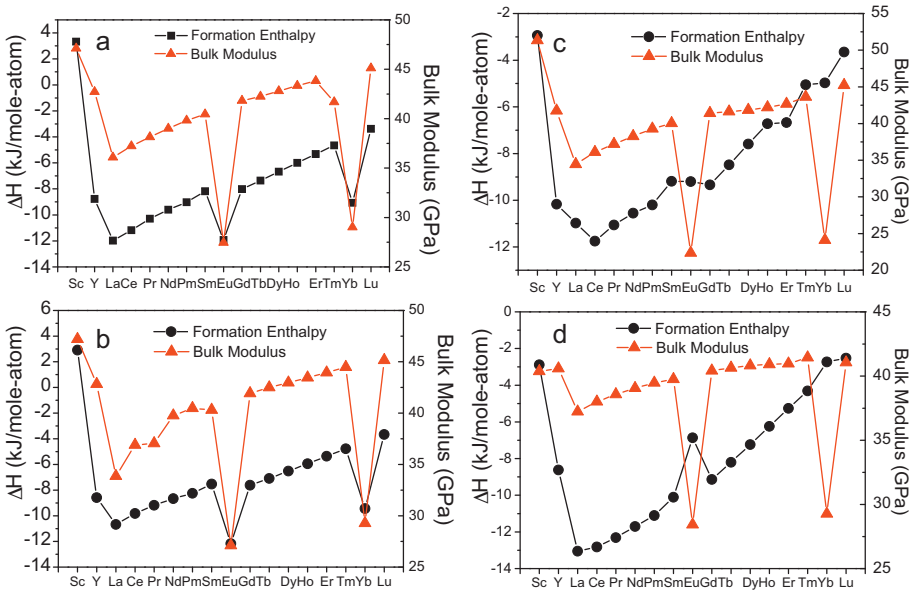

Fig. 3. The calculated enthalpies of formation and bulk moduli of (a) the $Mg_2RE.cF24$ compounds, (b) the $Mg_2RE.hP12$ compounds, (c) the MgRE.cP2 compounds and (d) the $Mg_3RE.cF16$ compounds.

3.1.4. Mg–Eu

From Fig. 1(i), $Mg_{17}Eu_2$.hP38, Mg_4Eu.hP90, Mg_2Eu.hP12 and MgEu.cP2 lie on the convex hull, and all of them are stable phases according to experiment investigation [35–37]. The formation enthalpies of the Mg_2Eu.hP12 and Mg_2Eu.hP12 are very close to each other, so Mg_2Eu.hP12 is a competed phase with Mg_2Eu.cF24 in the present calculations. The $MgEu_2$.tI6 lies above the convex hull by 1.32 kJ/mol of atom, which cannot be found in any literature. For the Mg_5Eu phase [35], the first-principles calculation cannot be applied due to its partial occupied atomic sites [36].

3.1.5. Mg–Gd

Fig. 1(j) exhibits that the Mg_3Gd.cF16 and MgGd.cP2 lie on the convex hull, and they are stable phases [35,36]. Mg_2Gd.cF24 and $MgGd_2$.tI6 lie above the convex hull by 1.21 kJ/mol of atom and 0.76 kJ/mol of atom, respectively. For the Mg_2Gd.cF24 phase, which is a stable phase in experiment [35,36], but the $MgGd_2$.tI6 phase is missing in the literature. In the Mg–Gd binary system, the Mg_5Gd has not been calculated, because the atomic sites are not fully occupied [36].

3.1.6. Mg–Tb, Mg–Dy, Mg–Ho, Mg–Er, Mg–Tm and Mg–Lu

From Fig. 1(k) and (l), the Mg_3Tb.cF16, MgTb.cP2, Mg_3Dy.cF16 and MgDy.cP2 are predicted as stable phases [35,36]. The $Mg_{24}Tb_5$.cI58 and $Mg_{24}Dy_5$.cI58 lie above the convex hull by 0.89 kJ/mol of atom and 0.68 kJ/mol of atom, respectively. And $MgRE_2$.tI6 is close to the convex hull in the present calculation. However, the $Mg_2RE.cF24$ performs a lower energy than that of $Mg_2RE.hP12$ in the two systems, the $Mg_2RE.hP12$ is stable phase observed in experiment [35]. From Table 1, the enthalpies of formation for the Mg_2Tb.cF24, Mg_2Tb.hP12, Mg_2Dy.cF24 and Mg_2Dy.hP12 are −7.4 kJ/mol of atom, −7.1 kJ/mol of atom, −6.7 kJ/mol of atom and −6.5 kJ/mol of atom, respectively. It is said that the enthalpies of formation for the $Mg_2RE.cF24$ and $Mg_2RE.hP12$ are much closed each other, and they are competing phases at 0 K. At the finite temperature, the entropy of the $Mg_2RE.cF24$ and $Mg_2RE.hP12$ will be different. So the apparent discrepancy can attribute to the entropy differences between the competing polymorphs in Mg_2RE, and the entropy of $Mg_2RE.hP12$ is larger than that of $Mg_2RE.cF24$, then reverse the phase stability.

We can discover, from Fig. 1(m) and (n), that $Mg_{24}Ho_5$.cI58, Mg_3Ho.cF16, MgHo.cP2, $Mg_{24}Er_5$.cI58, Mg_3Er.cF16 and MgEr.cP2 lie on the convex hull and $Mg_{24}Ho_5$.cI58, MgHo.cP2, $Mg_{24}Er_5$.cI58 and MgEr.cP2 are stable phases in experiment [35,36], the Mg_3Ho.cF16 and Mg_3Er.cF16 have not been reported by experiment. The enthalpies of formation of compete phases $Mg_2RE.cF24$ and $Mg_2RE.hP12$ are much closed; they lie above on the convex hull.

From Fig. 1(o), $Mg_{24}Tm_5$.cI58, Mg_3Tm.cF16, Mg_2Tm.hP12 and MgTm.cP2 lie on the convex hull, and $Mg_{24}Tm_5$.cI58, Mg_2Tm.hP12 and MgTm.cP2 are stable phases in experiment [35,36]. Mg_3Tm.cF16 has not been reported in experiment. From Fig. 1(q), $Mg_{24}Lu_5$.cI58, Mg_2Lu.hP12 and MgLu.cP2 lie on the convex hull, and they are stable phases in experiment [35,36].

3.1.7. Mg–Yb

The Mg–Yb system differs from the previous systems. There is only one stable phase known for the system, namely, Mg_2Yb.hP12 [35,36]. From Fig. 1(p), the Mg_2Yb.hP12 lies on the convex hull.

In the present calculations, the B2(CsCl.cP2)-type structure is stable phases in Mg–RE binary systems except in Mg–Yb system, and that is consistent with experiment [35]. The $D0_3(BiF_3$.cF16)-type structure is not reported in Mg–X (X = Sc, Y, Eu, Ho, Er, Tm, Yb and Lu), though, the present calculations indicates the existence of $D0_3(BiF_3$.cF16)-type structure in Mg–RE binary systems except for Mg_3Eu, Mg_3Yb and Mg_3Lu. Compared with experimental enthalpies of formation [38–41], the present calculated values are smaller in magnitude than experimental values. The present calculations can provide the correct thermodynamic properties from first-principles or can validate some theoretical values and illogically experimental data.

The variation trends of the equilibrium volumes for the individual family are shown in Fig. 2 and indicate "lanthanide contraction" effect. It should be noted that equilibrium volumes of the Sc and Y are smaller than that of lanthanide elements, so the deeply increase from Sc to La has been performed in Fig. 2. Compared with experimental equilibrium volumes, the agreement is well. And one can also find that the stable phases have the smallest equilibrium volume, such as the $Mg_3RE.cF16$ and MgRE.cP2. The equilibrium volumes of the $Mg_2RE.cF24$, $Mg_2RE.hP12$ and $Mg_2RE.tI6$ are closed

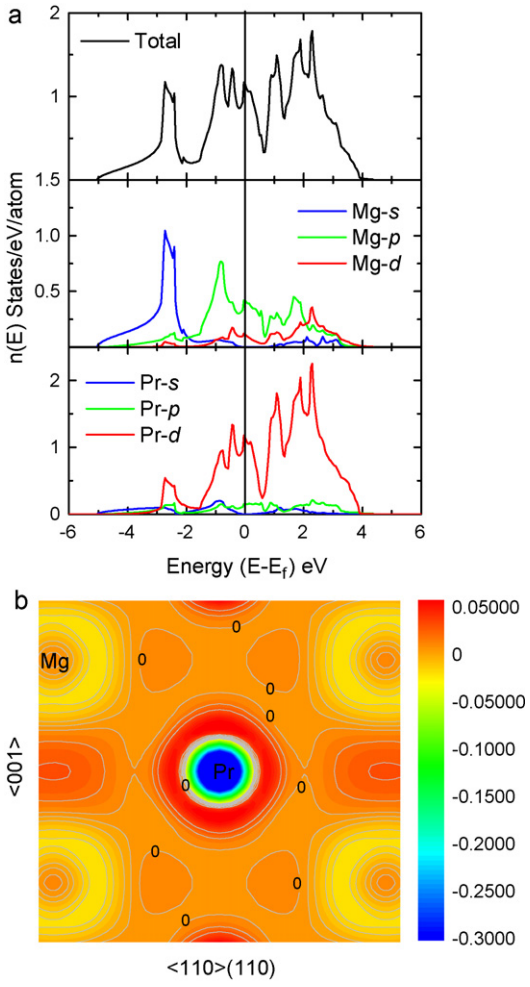

Fig. 4. (a) Electronic density of states, $n(E)$, for MgPr.cP2. (b) Distribution of bonding charge density in the (1 1 0) plane of MgPr.cP2 (the unit is eÅ^{-3}).

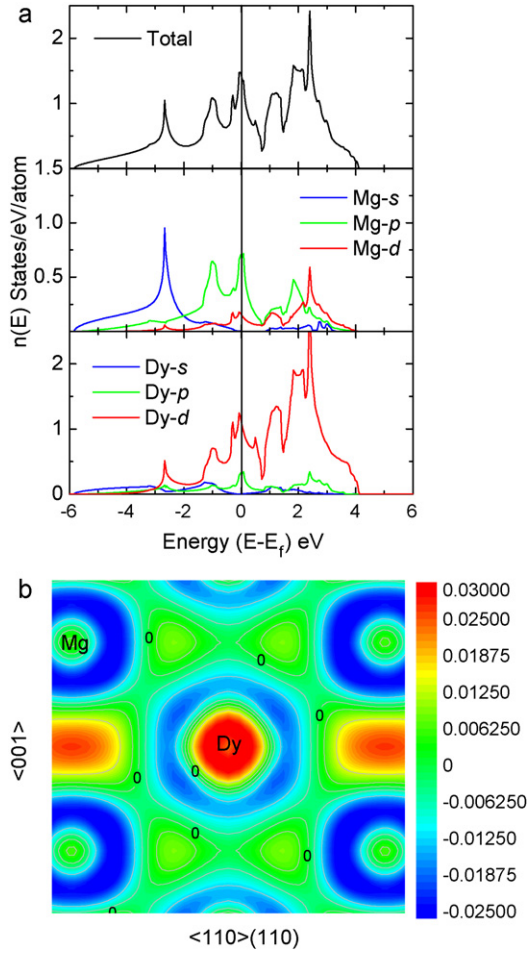

Fig. 5. (a) Electronic density of states, $n(E)$, for MgDy.cP2. (b) Distribution of bonding charge density in the 1 1 0 plane of MgDy.cP2 (the unit is eÅ^{-3}).

to each other and the enthalpies of formation of them approach closely. That is, among the same stoichiometric compounds, the smaller equilibrium volume mean stronger bonding in the system, and stronger bonding means more stable.

The first-principles calculated bulk moduli for the five families of compound are shown in Fig. 3, and the bulk moduli of the stable phases exhibited higher than others. This phenomenon is due to the atomic bonding between the atoms, the stronger bonding also means the bigger bulk modulus. From Fig. 3, it can be seen that the bulk moduli of the Mg_2Sc.cF24, Mg_2Sc.hP12, and MgSc.cP2 are bigger than that of other compounds with the same stoichiometric compounds. This means that the Sc is a effective addition in the Mg-based alloys. The bulk moduli of Mg–Y binary compounds are smaller that that of Mg–Sc binary compounds. From the calculated bulk moduli of the Mg–RE systems, the bulk moduli of the Mg–light RE are smaller than that of the Mg-heavy RE. The bulk moduli and enthalpies of formation of the Mg_2RE.cF24, Mg_2RE.hP12, MgRE.cP2, and Mg_3RE.cF16 are shown in Fig. 3(a)–(d), respectively. It can be seen from Fig. 3(a), the bulk moduli and enthalpies of formation increases with the atomic number increment. The trends of bulk moduli and enthalpies of formation of the Mg_2RE.cF24 are similar. For the Mg_2RE.hP12, MgRE.cP2, and Mg_3RE.cF16 compounds, the similar variation trends are also observed. However, it should be noted that the Mg_3Eu.cF16 phase is an unstable phase, and the formation enthalpy of the Mg_3Eu.cF16 is more positive, which can be found in Table 1, Figs. 1(i) and 3(d).

3.2. Electronic structure and bonding mechanism

In order to inspect the relationship between the electronic structure and the stability in Mg–RE intermetallics, the electronic densities of states and bonding charge densities for MgPr.cP2, MgDy.cP2, Mg_3Pr.cF16 and Mg_3Dy.cF16 have been calculated as examples for the light and heavy rare earth elements, respectively.

Figs. 4 and 5 display the calculated electronic DOS and bonding charge densities of MgPr.cP2 and MgDy.cP2, respectively. From Fig. 4(a), one can find out that the Fermi level lies about 1.8 eV to the right of the pseudo-gap minimum, that is, the bonding states are completely occupied. The total DOS at the Fermi level is $n(E_f)$ = 1.15 states/eV/atom. The bonding states are dominated by Mg-*s*, Mg-*p* and Pr-*d*, while the anti-bonding states are dominated by Pr-*d* and Mg-*p*. The hybridization occurred between Mg-*p* and Pr-*d* near the Fermi level. Both the Mg-*p* and Pr-*d* states are spread out on both sides of the Fermi level. In Fig. 4(b), the bonding charge density plotted in the (1 1 0) plane. The Pr atom loses electrons in its core, but a shielding electron buildup occurs around the electron-deficient core. Thereby, the total charge of the Pr atom is stand still. There is an electron enhancement between Mg atoms along the ⟨0 0 1⟩ direction, and a slightly increased electron density between the Pr atom and the enhanced region of the Mg atoms along ⟨1 1 0⟩ direction. All the evidence of the bonding charge densities indicates the covalent characteristic in the MgPr.cP2.

From Fig. 5(a), it can be seen that the electronic density of states for MgDy.cP2 are different from that of MgPr.cP2. The pseudo-gap minimum lies at the right of the Fermi level with 0.72 eV and this

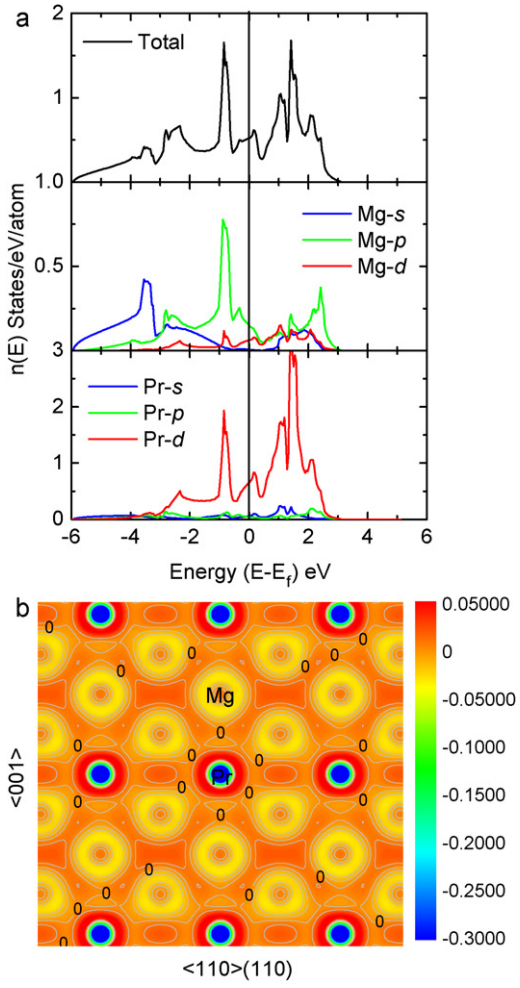

Fig. 6. (a) Electronic density of states, $n(E)$, for Mg_3Pr.cF16. (b) Distribution of bonding charge density in the (1 1 0) plane of Mg_3Pr.cF16 (the unit is eÅ^{-3}).

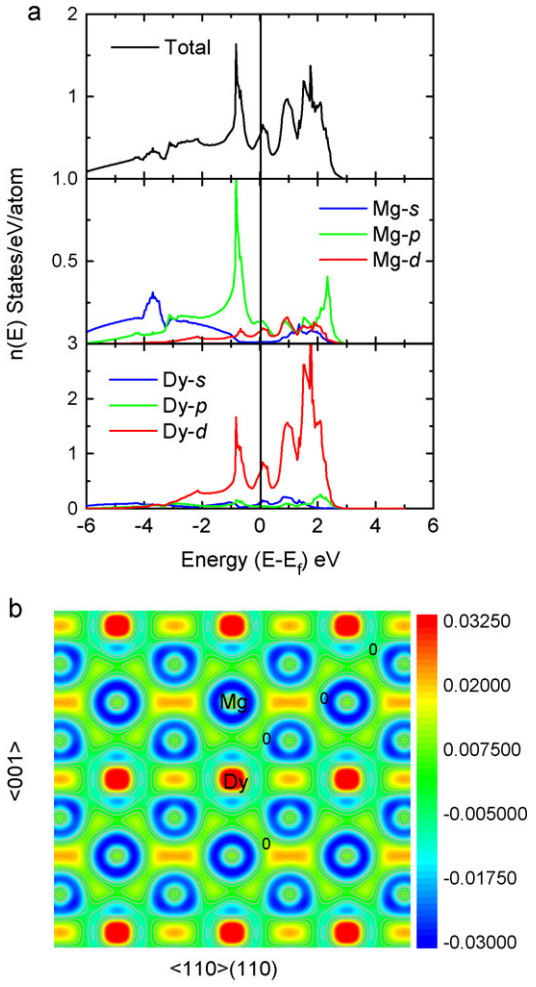

Fig. 7. (a) Electronic density of states, $n(E)$, for Mg_3Dy.cF16. (b) Distribution of bonding charge density in the (1 1 0) plane of Mg_3Pr.cF16 (the unit is eÅ^{-3}).

means that the bonding states are incompletely occupied. The total DOS at the Fermi level is $n(E_f)$ = 1.44 states/eV/atom, and which is larger than that of MgPr.cP2. Generally, the smaller $n(E_f)$ is, the more stable the compound is. So the MgPr.cP2 is more stable than MgDy.cP2 and which is in agreement with the results obtained from the enthalpies of formation, Similar to the DOS of MgPr.cP2, the bonding states of MgDy.cP2 are dominated by Mg-*s*, Mg-*p* and Dy-*d*, and the anti-bonding states are dominated by Dy-*d* and Mg-*p*. The Mg-*p* and Dy-*d* are hybridized near the Fermi level. In Fig. 5(b), the bonding charge density of MgDy.cP2 plotted in the (1 1 0) plane. Unlike that of MgPr.cP2, the Dy atom enhanced electrons in its core, and the electrons density decreases near the Dy atom. However, there is also an electron enhancement between Mg atoms along the ⟨0 0 1⟩ direction, and a slightly increased electron density between the Dy atom and the enhanced region of the Mg atoms along ⟨1 1 0⟩ direction. The bonding charge densities indicate the covalent characteristic in the MgDy.cP2.

The calculated electronic DOS and bonding charge densities of Mg_3Pr.cF16 and Mg_3Dy.cF16 are shown in Figs. 6 and 7, respectively. In Fig. 6(a), the Fermi level lies about 0.41 eV to the left of the pseudo-gap minimum, that is, the bonding states are incompletely occupied. The total DOS at the Fermi level is $n(E_f)$ = 0.52 states/eV/atom. The bonding states are dominated by Mg-*s*, Mg-*p* and Pr-*d*, while the anti-bonding states are dominated by Pr-*d*. Both the Mg-*p* and Pr-*d* states are spread out on both sides of the Fermi level. In Fig. 6(b), the bonding charge density is plotted in (1 1 0) plane. There is a significant delocalization of bonding charge in the interstitial region that resembles metallic bonding. And there is an electron enhancement along the ⟨1 1 1⟩ direction between the atoms and an electron decreased along ⟨0 0 1⟩ and ⟨1 1 0⟩ directions.

The electronic density of states for the Mg_3Dy.cF16 is similar to that of the Mg_3Pr.cF16. In Fig. 7(a), the Fermi level lies about 0.46 eV to the left of the pseudo-gap minimum, which revealed the incompletely occupied of bonding states The total DOS at the Fermi level is $n(E_f)$ = 0.53 states/eV/atom. The $n(E_f)$ of Mg_3Dy.cF16 is greater than that of Mg_3Pr.cF16, this also means the $D0_3$-Mg_3Pr is more stable than Mg_3Dy.cF16, and this is in good agreement with the present calculated enthalpies of formation. The bonding states are dominated by Mg-*s*, Mg-*p* and Dy-*d*, while the anti-bonding states are dominated by Mg-*p* and Dy-*d*. The hybridization occurred between Mg-*p* and Dy-*d* near the Fermi level. Both the Mg-*p* and Dy-*d* states are spread out on both sides of the Fermi level. In Fig. 7(b), the bonding charge density is plotted in (1 1 0) plane. There is a significant delocalization of bonding charge in the interstitial region that resembles metallic bonding.

4. Conclusions

In the present calculations, the density function theory has been employed to investigate the phase stability of the 17 Mg–RE (RE = Sc, Y, La–Lu) systems. The total enthalpies of formation for the 344 compounds of the Mg–RE binary systems have been calculated. The calculated equilibrium volumes and phase stabilities

at 0 K are in good agreement with experiment for most of systems considered. The calculated enthalpies of formation of the Mg–RE binary systems indicated that MgRE.cP2 existed in all of the Mg–RE system except in Mg–Yb system and Mg_3RE.cF16 existed in all of the Mg–RE except Mg–Eu, Mg–Yb and Mg–Lu systems. The electronic density of states and bonding charge densities of MgPr.cP2, MgDy.cP2, Mg_3Pr.cF16 and Mg_3Dy.cF16 has been calculated. The present calculations provide reasonable enthalpies of formation for Mg–RE binary systems and present valuable information for the thermodynamic database of Mg-based alloys.

Acknowledgements

This work is financially supported by the Key Program of National Natural Science Foundation of China (50831007), Natural Science Foundation of Guangxi (0832007), the Scientific Research Foundation of Guangxi University (Grant No. XBZ100022) and the State Key Laboratory of Powder Metallurgy of Central South University.

References

[1] H.E. Friedrich, B.L. Mordike, Magnesium Technology (Metallurgy, Design Data, Applications), Springer, Berlin, 2006.
[2] N. Stanford, D. Phelan, Acta Mater. 58 (2010) 3642.
[3] A. Datta, U.V. Waghmare, U. Ramamurty, Acta Mater. 56 (2008) 2531.
[4] Y.M. Zhu, A.J. Morton, J.F. Nie, Acta Mater. 58 (2010) 2936.
[5] J.X. Yi, B.Y. Tang, P. Chen, D.L. Li, L.M. Peng, W.J. Ding, J. Alloys Compd. 509 (2011) 669.
[6] A.K. Niessen, F.R. de Boer, R. Boom, P. de Chatel, W.C.M. Mattens, A.R. Miedema, Calphad 7 (1983) 51.
[7] Y.F. Ouyang, B.W. Zhang, S.Z. Liao, Z.P. Jin, Rare Met. Mater. Eng. 24 (1995) 32.
[8] W. Hu, H. Xu, X. Shu, X. Yuan, B. Gao, B. Zhang, J. Phys. D: Appl. Phys. 33 (2000) 711.
[9] A. Pisch, R. Schmid-Fetzer, G. Cacciamani, P. Riani, A. Saccone, R. Ferro, Z. Metallkd. 89 (1988) 474.
[10] O.B. Fabrichnaya, H.L. Lukas, G. Effenberg, F. Aldinger, Intermetallics 11 (2003) 1183.
[11] C. Guo, Z. Du, J. Alloys Compd. 385 (2004) 109.
[12] H. Zhang, Y. Wang, S. Shang, L.-Q. Chen, Z.-K. Liu, J Alloys Compd. 463 (2008) 294.
[13] C. Guo, Z. Du, J. Alloys Compd. 399 (2005) 183.
[14] S. Gorsse, C.R. Hutchinson, B. Chevalier, J.F. Nie, J. Alloys Compd. 392 (2005) 253.
[15] X.M. Tao, H. Wang, W.J. Zhu, H.S. Liu, Y.F. Ouyang, Z.P. Jin, Calphad 32 (2008) 462.
[16] G. Cacciamani, S. De Negri, A. Saccone, R. Ferro, Intermetallics 11 (2003) 1135.
[17] C. Guo, Z. Du, J. Alloys Compd. 422 (2006) 102.
[18] G. Cacciamani, A. Saccone, S. De Negri, R. Ferro, J. Phase Equilib. 23 (2002) 38.
[19] Z. Du, H. Liu, G. Ling, J. Alloys Compd. 373 (2004) 151.
[20] X. Zhang, D. Kevorkov, M.O. Pekguleryuz, J. Alloys Compd. 501 (2010) 366.
[21] X. Zhang, D. Kevorkov, M.O. Pekguleryuz, J. Alloys Compd. 475 (2009) 361.
[22] D.W. Zhou, P. Peng, J.S. Liu, J. Alloys Compd. 428 (2007) 316.
[23] H. Zhang, S. Shang, J.E. Saal, A. Saengdeejing, Y. Wang, L.Q. Chen, Z.-K. Liu, Intermetallics 17 (2009) 878.
[24] A. Berche, F. Marinelli, J. Rogez, M.-C. Record, Thermochim. Acta 499 (2010) 65.
[25] Y.F. Wang, W.B. Zhang, Z.Z. Wang, et al., Comput. Mater. Sci. 41 (2007) 78.
[26] P. Chen, D.L. Li, J.-X. Yi, L. Wen, B.-Y. Tang, L.-M. Peng, W.-J. Ding, Solid State Sci. 11 (2009) 2156.
[27] P.E. Blöchl, Phys. Rev. B 50 (1994) 17953.
[28] G. Kresse, J. Joubert, Phys. Rev. B 59 (1999) 1758.
[29] G. Kresse, J. Furthmuller, Phys. Rev. B 54 (1996) 11169.
[30] G. Kresse, J. Furthmuller, Comput. Mater. Sci. 6 (1996) 15.
[31] J.P. Perdew, Y. Wang, Phys. Rev. B 45 (1992) 13244.
[32] J.P. Perdew, J.A. Chevary, S.H. Vosko, et al., Phys. Rev. B 46 (1992) 6671.
[33] H.J. Monkhorst, J.D. Pack, Phys. Rev. B 13 (1972) 5188.
[34] P. Vinet, J.H. Rose, J. Ferrante, J.R. Smith, J. Phys.: Condens. Matter 1 (1989) 1941.
[35] T.B. Massalski et al., Binary Alloy Phase Diagrams, ASM International, Materials Park, OH, 1995.
[36] P. Villars, L.D. Calvert, Pearson's Handbook of Crystallographic Data for Intermetallic Phases, vol. 1–4, ASM International, Materials Park, OH, 1991.
[37] W. Klemm, H. Kock, W. Muhlpfordt, Angew. Chem. Int. 3 (1964) 704.
[38] J.F. Smith, D. Bailey, D.B. Novotny, J.E. Davison, Acta Metall. 13 (1965) 558.
[39] I.N. Pyagai, E.Z. Khasanova, A.V. Vakhobov, O.V. Zhikhareva, Dokl. Akad. Nauk. Tadzh. SSR 33 (1990) 602.
[40] F. Bonhomme, K. Yvon, J. Alloys Compd. 232 (1996) 271.
[41] J.E. Pahlman, J.F. Smith, Metall. Trans. 3 (1972) 2423.